Tunneling in Fermi Systems with Quadratic Band Crossing Points

Ipsita Mandal
Faculty of Science and Technology, University of Stavanger, 4036 Stavanger, Norway

We investigate the tunneling of quasiparticles through a potential barrier of finite height and width, in a system with a band structure consisting of a quadratic band crossing point (QBCP). We compute the results of the transmission coefficient at various incident angles, and also the conductivity and the Fano factor. We discuss the distinguishing signatures of these transport properties in comparison with other semimetals, as well as electrons in normal metals.

CONTENTS

I. INTRODUCTION

Multiband fermionic systems may exhibit a band crossing point in the Brillouin zone where two or more bands cross. If the chemical potential is adjusted to lie exactly at that point, the Fermi surface shrinks to a Fermi node. The most famous example of such a Fermi node is the case of a linear band crossing, whose low energy properties are described by Dirac fermions, and are conspicuous in systems like nodal superconductors and graphene. In this paper, we consider systems with a quadratic band crossing point (QBCP) somewhere in their two-dimensional (2d)[1–3] or three-dimensional (3d)[4–6] Brillouin zones. 2d QBCPs can be realised in checkerboard[1] (at 1/2 filling), Kagome[1] (at 1/3 filling), and Lieb[2] lattices. On the other hand, pyrochlore iridates $A_2Ir_2O_7$ (A is a lanthanide element[7,8]) have been shown to host a 3d QBCP. Such bandstructures have also been realised that in 3d gapless semiconductors in the presence of a sufficiently strong spin-orbit coupling,[9] such that the resulting model of a semimetal is indeed relevant for materials like gray tin (α-Sn) and mercury telluride (HgTe). These systems are also known as "Luttinger semimetals"[10] due to the fact that the low-energy fermionic degrees of freedom are captured by the Luttinger Hamiltonian of inverted band-gap semiconductors.[11,12]

Our aim is to compute the tunneling coefficients and other transport characteristics when the quasiparticles of the QBCP semimetals are subjected to a potential barrier of finite strength and width along one direction, which is chosen to be the x-axis. This scenario is represented in the cartoon in Fig. 1. Our results will show how these transport characteristics are significantly different from those in normal metals, due to the presence of multiple bands. We will also compare their features with those of other semimetals like graphene, bilayer graphene and three-band pseudospin-1 systems.

The paper is organized as follows. In Sec. II, we study the 2d QBCPs, while Sec. III deals with the 3d QBCP case. We compare our findings with the results for some other known bandstructures in Sec. IV. Finally, we end with a summary and outlook in Sec. V.

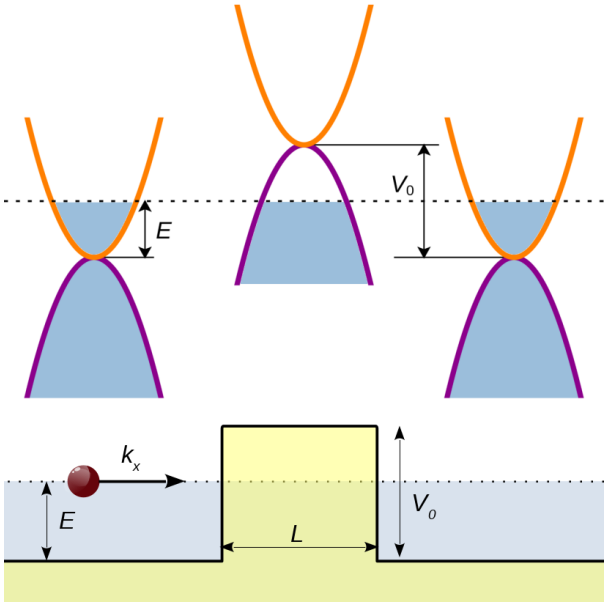

FIG. 1. Tunneling through a potential barrier in a QBCP material. The upper panel shows the schematic diagrams of the spectrum of quasiparticles about a QBCP, with respect to a potential barrier in the x-direction. The lower panel represents the schematic diagram of the transport across the potential barrier. The Fermi level (indicated by dotted lines) lies in the conduction band outside the barrier, and in the valence band inside it. The blue fillings indicate occupied states.

II. 2D MODEL

For a 2d system, the particle-hole symmetric QBCP is described by the Hamiltonian:[1]

$$\mathcal{H}_{2d}^{kin}(k_x, k_y) = \frac{\hbar^2}{2\,m}\Big[\,2\,k_x\,k_y\,\sigma_x + \left(k_y^2 - k_x^2\right)\sigma_z\,\Big] \tag{2.1}$$

in the momentum space, with eigenvalues

$$\varepsilon_{2d}^{\pm}(k_x, k_y) = \pm\frac{\hbar^2\left(k_x^2 + k_y^2\right)}{2\,m}, \tag{2.2}$$

where the "+" and "−" signs, as usual, refer to the conduction and valence bands respectively. The corresponding eigenvectors are given by:

$$\Psi_+ = \frac{1}{\sqrt{k_x^2 + k_y^2}}\{k_y, k_x\}\,,\ \text{and}\ \Psi_- = \frac{1}{\sqrt{k_x^2 + k_y^2}}\{-k_x, k_y\}, \tag{2.3}$$

respectively.

The 2d system is modulated by a square electric potential barrier of height V_0 and width L, giving rise to an x-dependent potential energy function:

$$V(x) = \begin{cases} V_0 & \text{for } 0 < x < L \\ 0 & \text{otherwise}\,. \end{cases} \tag{2.4}$$

Hence, we need to consider the total Hamiltonian:

$$\mathcal{H}_{2d}^{tot} = \mathcal{H}_{2d}^{kin}(-\mathrm{i}\,\partial_x, -\mathrm{i}\,\partial_y) + V(x) \tag{2.5}$$

in position space. We choose the x-axis along the transport direction, and place the chemical potential at an energy $E > 0$ in the region outside the potential barrier. The Fermi energy E can in general be tuned by chemical doping or a gate voltage.

A. Formalism

For a material of a sufficiently large transverse dimension W, the boundary conditions should be irrelevant for the bulk response, and we use this freedom to simplify the calculation. Here, on a physical wavefunciton $\Psi^{\rm tot}$ we impose periodic boundary conditions:

$$\Psi^{\rm tot}(x,W) = \Psi^{\rm tot}(x,0)\,. \tag{2.6}$$

The transverse momentum k_y is conserved, and it is quantized due to the periodicity in the transverse width W, and hence takes the form:

$$k_y = \frac{2\,\pi\,n}{W} \equiv q_n\,, \tag{2.7}$$

where $n \in \mathbb{Z}$. For the longitudinal direction, we seek plane wave solutions of the form $e^{{\rm i}\,k_x x}$. Then the full wavefunction is given by:

$$\Psi^{\rm tot}(x,y,n) = {\rm const.} \times \Psi_n(x)\, e^{{\rm i}\,q_n y}\,, \tag{2.8}$$

For any mode of given transverse momentum component k_y, we can determine the x-component of the wavevectors of the incoming, reflected, and transmitted waves (denoted by k_ℓ), by solving $\varepsilon^{\pm}_{2d}(k_x,n) = \pm\frac{\hbar^2\left(k_\ell^2+q_n^2\right)}{2\,m}$. In the regions $x<0$ and $x>L$, we have only propagating modes (k_ℓ is real), while the x-components in the scattering region (denoted by $\tilde{k}$), are given by $\tilde{k}^2 = \frac{2\,m\,|E-V_0|}{\hbar^2} - q_n^2$, and may be propagating (imaginary part of $\tilde{k}$ is zero) or evanescent (imaginary part of $\tilde{k}$ is nonzero).

We will follow the procedure outlined in Refs. 13 and 14 to compute the transport coefficients. We consider the transport of positive energy states (Ψ_+) corresponding to electron-like particles. The transport of hole-like excitations (Ψ_-) will be similar. Hence, the Fermi level outside the potential barrier is adjusted to a value $E = \varepsilon^{+}_{2d}(k_x,k_y)$. Such a scattering state $\Psi_{n,+}$, in the mode labeled by n, is constructed from the states:

$$\begin{aligned}
\Psi_n(x) &= \begin{cases} \phi_L & \text{for } x<0\,, \\ \phi_M & \text{for } 0<x<L\,, \\ \phi_R & \text{for } x>L\,, \end{cases} \\
\phi_L &= \frac{\Psi_+(k_\ell,q_n)\,e^{{\rm i}\,k_\ell x} + r_n\,\Psi_+(-k_\ell,q_n)\,e^{-{\rm i}\,k_\ell x}}{\sqrt{\mathcal{V}(k_\ell,n)}}\,, \\
\phi_M &= \left[\alpha_n\,\Psi_+(\tilde{k},q_n)\,e^{{\rm i}\,\tilde{k}\,x} + \beta_n\,\Psi_+(-\tilde{k},q_n)\,e^{-{\rm i}\,\tilde{k}\,x}\right]\Theta\left(E-V_0\right) + \left[\alpha_n\,\Psi_-(\tilde{k},q_n)\,e^{{\rm i}\,\tilde{k}\,x} + \beta_n\,\Psi_-(-\tilde{k},q_n)\,e^{-{\rm i}\,\tilde{k}\,x}\right]\Theta\left(V_0-E\right), \\
\phi_R &= t_n\,\Psi_+(k_\ell,q_n)\,\frac{e^{{\rm i}\,k_\ell(x-L)}}{\sqrt{\mathcal{V}(k_\ell,n)}}\,, \\
\mathcal{V}(k_\ell,n) &\equiv \left|\partial_{k_\ell}\varepsilon_+(k_\ell,n)\right| = \frac{\hbar^2 k_\ell}{m}\,, \quad k_\ell = \sqrt{\frac{2\,m\,E}{\hbar^2} - q_n^2}\,, \quad \tilde{k} = \sqrt{\frac{2\,m\,|E-V_0|}{\hbar^2} - q_n^2}\,,
\end{aligned} \tag{2.9}$$

where we have used the velocity $\mathcal{V}(k_\ell,n)$ to normalize the incident, reflected and transmitted plane waves. Note that for $V_0 > E$, the Fermi level within the potential barrier lies within the valence band, and we must use the valence band wavefunctions in that region.

The boundary conditions can be obtained by integrating the equation $\mathcal{H}^{tot}_{2d}\,\Psi^{\rm tot} = E\,\Psi^{\rm tot}$ over a small interval in the x-direction around the points $x=0$ and $x=L$. The results are that the two components of the wavefunction be continuous at the boundaries. These conditions are sufficient to guarantee the continuity of the current flux along the x-direction. In particular, the reflection and transmission amplitudes r_n, t_n, and the two coefficients (α_n,β_n), are determined from these boundary conditions. This mode-matching procedure gives us:

$$t_n(E,V_0) = \begin{cases} -\frac{2\,{\rm i}\,\tilde{k}\,k_\ell\,q_n^2}{\left(\tilde{k}^2\,k_\ell^2+q_n^4\right)\sin\left(\tilde{k}L\right)-2\,{\rm i}\,\tilde{k}\,k_\ell\,q_n^2\cos\left(\tilde{k}L\right)} & \text{for } E<V_0 \\ \frac{2\,{\rm i}\,\tilde{k}\,k_\ell}{\left(\tilde{k}^2+k_\ell^2\right)\sin\left(\tilde{k}L\right)+2\,{\rm i}\,\tilde{k}\;k_\ell\cos\left(\tilde{k}L\right)} & \text{for } E>V_0\,. \end{cases} \tag{2.10}$$

The transmission coefficient at an energy E is given by

$$T(E, V_0, \phi) = |t_n(E, V_0)|^2 \,, \text{ where } \phi = \tan^{-1}\left(\frac{q_n}{k_\ell}\right) \tag{2.11}$$

is the incident angle of the incoming wave.

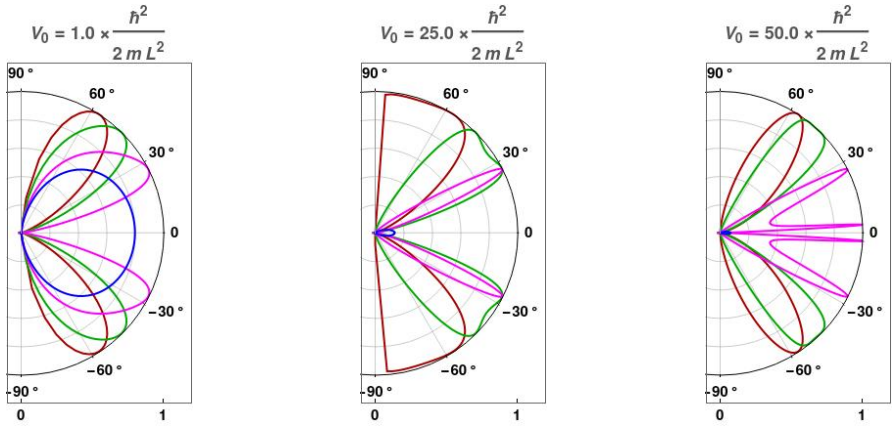

(a) (b) (c)

FIG. 2. 2d QBCP: The polar plots show the transmission coefficient $T(E, V_0, \phi)\big|_{E \le V_0}$ as functions of the incident angle ϕ for the parameters $E = 0.3\, V_0$ (red), $E = 0.5\, V_0$ (green), $E = 0.8\, V_0$ (magenta) and $E = 1.0\, V_0$ (blue).

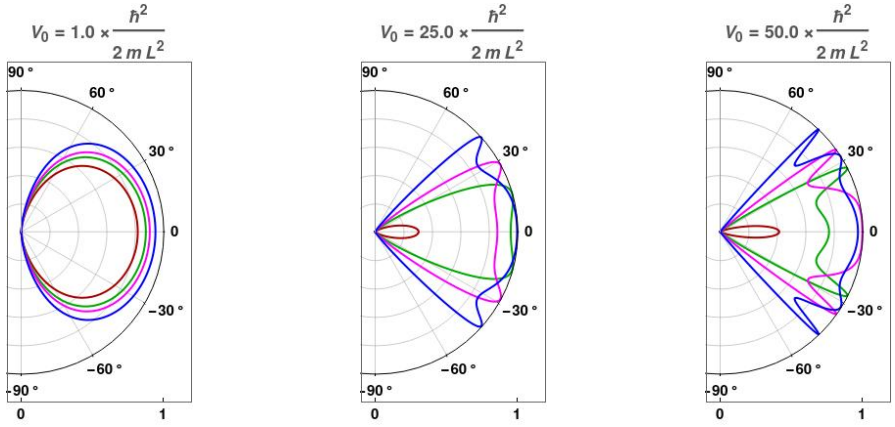

(a) (b) (c)

FIG. 3. 2d QBCP: The polar plots show the transmission coefficient $T(E, V_0, \phi)\big|_{E > V_0}$ as functions of the incident angle ϕ for the parameters $E = 1.1\, V_0$ (red), $E = 1.5\, V_0$ (green), $E = 1.8\, V_0$ (magenta) and $E = 2.5\, V_0$ (blue).

B. Transmission coefficient, conductivity and Fano factor

Let us assume W to be very large such that q_n can effectively be treated as a continuous variable. We then numerically compute $T(E, \phi)$.

Using $k_\ell = \sqrt{\frac{2mE}{\hbar^2}}\cos\phi\,, \quad n = \frac{W\sqrt{2mE}}{h}\sin\phi\,, \quad dn = \frac{2\,W\sqrt{2mE}}{h}\cos\phi\, d\phi$, in the zero-temperature limit and for a

Preprints (www.preprints.org) | NOT PEER-REVIEWED | Posted: 5 June 2020 doi:10.20944/preprints202006.0051.v1

Peer-reviewed version available at Annals of Physics 2020, 419, 168235; doi:10.1016/j.aop.2020.168235

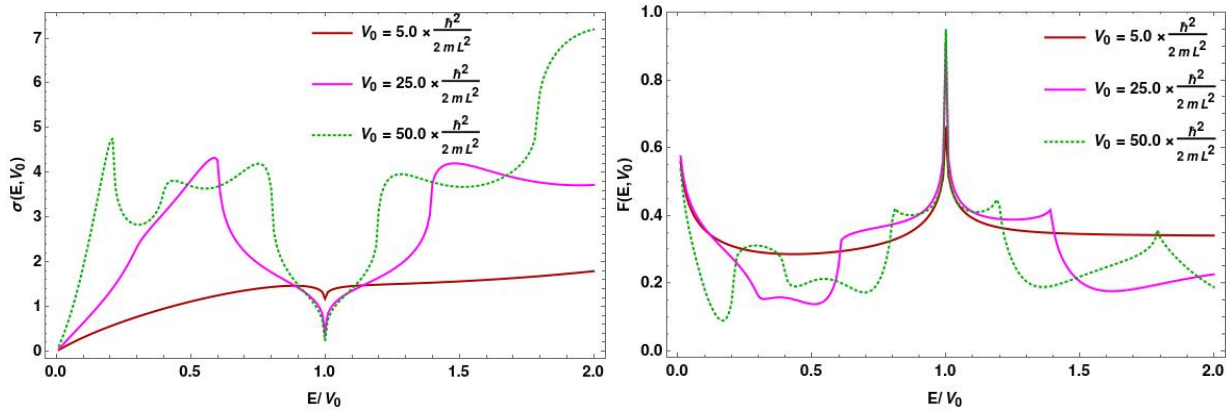

(a) (b)

FIG. 4. 2d QBCP: Plots of the (a) conductivity (σ in units of 2π), and (b) Fano factor (F), as functions of E/V_0, for various values of V_0.

small applied voltage, the conductance is given by:[15]

$$G(E,V_0) = \frac{e^2}{h}\sum_n |t_n|^2 \to \frac{e^2}{h}\int |t_n(E)|^2\, dn = \frac{e^2\, W\sqrt{2\,m\,E}}{h^2}\int_{-\frac{\pi}{2}}^{\frac{\pi}{2}} T(E,V_0,\phi)\cos\phi\, d\phi\,. \tag{2.12}$$

Therefore, the conductivity is given by:

$$\sigma(E,V_0) = \frac{L}{W}\frac{G(E,V_0)}{e^2/h} = 2\,\pi\sqrt{\frac{E}{\hbar^2/\left(2\,mL^2\right)}}\int_{-\frac{\pi}{2}}^{\frac{\pi}{2}} T(E,V_0,\phi)\cos\phi\, d\phi\,. \tag{2.13}$$

Shot noise is the measure of the fluctuations of the current away from their average value. The zero-temperature shot noise is given by:[15]

$$\mathcal{S}(E,V_0) = \frac{2\,e^2\,\Phi}{h}\sum_n |t_n|^2\,|r_n|^2 \to \frac{e^3\,\Phi\,W\sqrt{\frac{E}{\hbar^2/(2\,mL^2)}}}{\pi\,h\,L}\int_{-\frac{\pi}{2}}^{\frac{\pi}{2}} T(E,V_0,\phi)\left[1-T(E,V_0,\phi)\right]\, d\phi\,, \tag{2.14}$$

where Φ is the applied voltage, and is characterized by the Fano factor:

$$F(E,V_0) = \frac{\int_{-\frac{\pi}{2}}^{\frac{\pi}{2}} T(E,V_0,\phi)\, d\phi}{\int_{-\frac{\pi}{2}}^{\frac{\pi}{2}} T(E,V_0,\phi)\left[1-T(E,V_0,\phi)\right]\, d\phi}\,. \tag{2.15}$$

We express E and V_0 in units of $\frac{\hbar^2}{2\,mL^2}$, and study the behaviour of $T(E,V_0,\phi)$, $\sigma(E,V_0)$ and $F(E,V_0)$. Figs. 2 and 3 show the polar plots of $T(E,V_0,\phi)$ as a function of the incident angle ϕ, for the cases $E \le V_0$ and $E > V_0$ respectively. From the expression of transmission coefficient in Eq. (4.1), it is clear that the transmission is zero at normal incidence ($\phi = 0$), as long as $E < V_0$. Hence, we do not have a Klein tunneling analogue in the 2d QBCP, unlike graphene[16] or three-band pseudospin-1 Dirac-Weyl systems.[17,18] However, we still have the resonance conditions $\tilde{k}\,L = \pi N$, $N \in \mathbb{Z}$, under which the barrier becomes transparent ($T = 1$). In Fig. 4, we illustrate the conductivity $\sigma(E,V_0)$ and the Fano factor $F(E,V_0)$, as functions of E/V_0, for some values of V_0.

III. 3D MODEL

We consider a model for 3d QBCP semimetals, where the low energy bands form a four-dimensional representation of the lattice symmetry group.[6] Then the standard $(\mathbf{k}\cdot\mathbf{p})$ Hamiltonian for the particle-hole symmetric system can be written by using the five 4×4 Euclidean Dirac matrices Γ_a as:[12,19]

$$\mathcal{H}_{3d}^{kin}(k_x,k_y,k_z) = \frac{\hbar^2}{2\,m}\sum_{a=1}^{5} d_a(\mathbf{k})\;\Gamma_a\,. \tag{3.1}$$

The Γ_a's form one of the (two possible) irreducible, four-dimensional Hermitian representations of the five-component Clifford algebra defined by the anticommutator $\{\Gamma_a, \Gamma_b\} = 2\,\delta_{ab}$. The five anticommuting gamma-matrices can always be chosen such that three are real and two are imaginary.[12,20] In the representation used here, $(\Gamma_1, \Gamma_2, \Gamma_3)$ are real and (Γ_1, Γ_3) are imaginary:[12]

$$\Gamma_1 = \sigma_3 \otimes \sigma_2\,, \quad \Gamma_2 = \sigma_3 \otimes \sigma_1\,, \quad \Gamma_3 = \sigma_2 \otimes \sigma_0\,, \quad \Gamma_4 = \sigma_1 \otimes \sigma_0\,, \quad \Gamma_5 = \sigma_3 \otimes \sigma_3\,. \tag{3.2}$$

The five functions $d_a(\mathbf{k})$ are the real $\ell = 2$ spherical harmonics, with the following structure:

$$\begin{aligned} d_1(\mathbf{k}) &= -\sqrt{3}\,k_y\,k_z\,,\ d_2(\mathbf{k}) = -\sqrt{3}\,k_x\,k_z\,,\ d_3(\mathbf{k}) = -\sqrt{3}\,k_x\,k_y, \\ d_4(\mathbf{k}) &= \frac{-\sqrt{3}}{2}(k_x^2 - k_y^2)\,,\ d_5(\mathbf{k}) = \frac{-1}{2}\left(2\,k_z^2 - k_x^2 - k_y^2\right). \end{aligned} \tag{3.3}$$

The energy eigenvalues are

$$\varepsilon_{3d}^{\pm}(k_x, k_y, k_z) = \pm\frac{\hbar^2\left(k_x^2 + k_y^2 + k_z^2\right)}{2\,m}, \tag{3.4}$$

where the "+" and "−" signs, as usual, refer to the conduction and valence bands. Each of these bands are doubly degenerate.

A set of orthogonal eigenvectors are given by:

$$\begin{aligned} \Psi_{+,1}^T &= \left\{-\frac{(k_x + \mathrm{i}\,k_y)\,(k + k_z)}{(k_x - \mathrm{i}\,k_y)^2}, \frac{\mathrm{i}\,(k + 3\,k_z)}{\sqrt{3}\,(k_x - \mathrm{i}\,k_y)}, -\frac{\mathrm{i}\left(-2\,k_z\,(k + k_z) + k_x^2 + k_y^2\right)}{\sqrt{3}\,(k_x - \mathrm{i}\,k_y)^2}, 1\right\}, \\ \Psi_{+,2}^T &= \left\{\frac{(k_x + \mathrm{i}\,k_y)\,(k - k_z)}{(k_x - \mathrm{i}\,k_y)^2}, -\frac{\mathrm{i}\,(k - 3\,k_z)}{\sqrt{3}\,(k_x - \mathrm{i}\,k_y)}, -\frac{\mathrm{i}\left(2\,k_z\,(k - k_z) + k_x^2 + k_y^2\right)}{\sqrt{3}\,(k_x - \mathrm{i}\,k_y)^2}, 1\right\}, \\ \Psi_{-,1}^T &= \left\{-\frac{\mathrm{i}\,(k + k_z)}{\sqrt{3}\,(k_x - \mathrm{i}\,k_y)}, \frac{k - k_z}{k_x + \mathrm{i}\,k_y}, 1, -\frac{\mathrm{i}\left(2\,k_z\,(k_z - k) + k_x^2 + k_y^2\right)}{\sqrt{3}\,(k_x + \mathrm{i}\,k_y)^2}\right\}, \\ \Psi_{-,2}^T &= \left\{\frac{\mathrm{i}\,(k - k_z)}{\sqrt{3}\,(k_x - \mathrm{i}\,k_y)}, -\frac{k + k_z}{k_x + \mathrm{i}\,k_y}, 1, -\frac{\mathrm{i}\left(2\,k_z\,(k + k_z) + k_x^2 + k_y^2\right)}{\sqrt{3}\,(k_x + \mathrm{i}\,k_y)^2}\right\}, \end{aligned} \tag{3.5}$$

where $k = \sqrt{k_x^2 + k_y^2 + k_z^2}$, and the "+" ("−") indicates an eigenvector corresponding to the positive (negative) eigenvalue.

The 3d system is modulated by a square electric potential barrier of height V_0 and width L, as described in Eq. (2.4). Here, we need to consider the total Hamiltonian:

$$\mathcal{H}_{3d}^{tot} = \mathcal{H}_{3d}^{kin}(-\mathrm{i}\,\partial_x, -\mathrm{i}\,\partial_y, -\mathrm{i}\,\partial_z) + V(x) \tag{3.6}$$

in position space. As before, we choose the x-axis along the transport direction, and place the chemical potential at an energy $E > 0$ in the region outside the potential barrier.

A. Formalism

We consider the tunneling in a slab of height and width W. Again, we assume that the material has a sufficiently large width W along each of the two transverse directions, such that the boundary conditions are irrelevant for the bulk response, and impose the periodic boundary conditions:

$$\tilde{\Psi}^{\mathrm{tot}}(x, 0, z) = \tilde{\Psi}^{\mathrm{tot}}(x, W, z)\,, \quad \tilde{\Psi}^{\mathrm{tot}}(x, y, 0) = \tilde{\Psi}^{\mathrm{tot}}(x, y, W)\,. \tag{3.7}$$

The transverse momentum $\mathbf{k}_\perp = (k_y, k_z)$ is conserved, and its components are quantized. Due to periodicity, we conclude that:

$$k_y = \frac{2\,\pi\,n_y}{W} \equiv q_{n_y}\,, \quad k_z = \frac{2\,\pi\,n_z}{W} \equiv q_{n_z}\,, \tag{3.8}$$

where $(n_x, n_y) \in \mathbb{Z}$. For the longitudinal direction (along the x-axis), we seek plane wave solutions of the form $e^{\mathrm{i}\, k_x x}$. Then the full wavefunction is given by:

$$\tilde{\Psi}^{\rm tot}(x,y,z,\mathbf{n}) = \text{const.} \times \tilde{\Psi}_{\mathbf{n}}(x)\, e^{\mathrm{i}\left(q_{n_y} y + q_{n_z} z\right)}\,, \tag{3.9}$$

with

$$\mathbf{n} = (n_y, n_z)\,. \tag{3.10}$$

For any mode of given transverse momentum component $\mathbf{k}_\perp$, we can determine the x-component of the wavevectors of the incoming, reflected, and transmitted waves (denoted by k_ℓ), by solving $\varepsilon^{\pm}_{3d}(k_x, \mathbf{n}) = \pm\frac{\hbar^2\left(k_\ell^2 + {\mathbf{k}_\perp}^2\right)}{2\,m}$. In the regions $x<0$ and $x>L$, we have only propagating modes (k_ℓ is real), while the x-components in the scattering region (denoted by $\tilde{k}$), are given by $\tilde{k}^2 = \frac{2\,m\,|E-V_0|}{\hbar^2} - {\mathbf{k}_\perp}^2$, and may be propagating ($\tilde{k}$ is real) or evanescent ($\tilde{k}$ is imaginary).

We will follow the same procedure as described for the 2d QBCP. Again, without any loss of generality, we consider the transport of one of the degenerate positive energy states ($\Psi_{+,1}$) corresponding to electron-like particles, with the Fermi level outside the potential barrier being adjusted to a value $E = \varepsilon^{+}_{3d}(k_x, k_y, k_z)$. In this case, a scattering state $\tilde{\Psi}_{\mathbf{n}}$, in the mode labeled by $\mathbf{n}$, is constructed from the states:

$$\begin{aligned}
\tilde{\Psi}_{\mathbf{n}}(x) &= \begin{cases} \tilde{\phi}_L & \text{for } x<0\,, \\ \tilde{\phi}_M & \text{for } 0<x<L\,, \\ \tilde{\phi}_R & \text{for } x>L\,, \end{cases} \\
\tilde{\phi}_L &= \frac{\Psi_{+,1}(k_\ell, q_{n_y}, q_{n_z})\, e^{\mathrm{i}\, k_\ell x} + \sum\limits_{s=1,2} r_{\mathbf{n},s}\, \Psi_{+,s}(-k_\ell, q_{n_y}, q_{n_z})\, e^{-\mathrm{i}\, k_\ell x}}{\sqrt{\tilde{\mathcal{V}}(k_\ell, \mathbf{n})}}\,, \\
\tilde{\phi}_M &= \Big[\sum_{s=1,2} \alpha_{\mathbf{n},s}\, \Psi_{+,s}(\tilde{k}, q_{n_y}, q_{n_z})\, e^{\mathrm{i}\,\tilde{k}\,x} + \sum_{s=1,2} \beta_{\mathbf{n},s}\, \Psi_{+,s}(-\tilde{k}, q_{n_y}, q_{n_z})\, e^{-\mathrm{i}\,\tilde{k}\,x}\Big]\Theta\left(E - V_0\right) \\
&\quad + \Big[\sum_{s=1,2} \alpha_{\mathbf{n},s}\, \Psi_{-,s}(\tilde{k}, q_{n_y}, q_{n_z})\, e^{\mathrm{i}\,\tilde{k}\,x} + \sum_{s=1,2} \beta_{\mathbf{n},s}\, \Psi_{-,s}(-\tilde{k}, q_{n_y}, q_{n_z})\, e^{-\mathrm{i}\,\tilde{k}\,x}\Big]\Theta\left(V_0 - E\right)\,, \\
\tilde{\phi}_R &= \frac{\sum\limits_{s=1,2} t_{\mathbf{n},s}\, \Psi_{+,s}(k_\ell, q_{n_y}, q_{n_z})}{\sqrt{\tilde{\mathcal{V}}(k_\ell, \mathbf{n})}}\, e^{\mathrm{i}\, k_\ell (x-L)}, \\
\tilde{\mathcal{V}}(k_\ell, \mathbf{n}) &\equiv \left|\partial_{k_\ell} \varepsilon^{+}_{3d}(k_\ell, \mathbf{n})\right| = \frac{\hbar^2 k_\ell}{m}\,, \quad k_\ell = \sqrt{\frac{2\,m\,E}{\hbar^2} - q_{n_y}^2 - q_{n_z}^2}\,, \quad \tilde{k} = \sqrt{\frac{2\,m\,|E-V_0|}{\hbar^2} - q_{n_y}^2 - q_{n_z}^2}\,,
\end{aligned} \tag{3.11}$$

where we have used the velocity $\tilde{\mathcal{V}}(k_\ell, \mathbf{n})$ to normalize the incident, reflected and transmitted plane waves. Note that for $V_0 > E$, the Fermi level within the potential barrier lies within the valence band, and we must use the valence band wavefunctions in that region.

The usual mode-matching procedure at $x=0$ and $x=L$ gives us:

$$\begin{aligned}
t_{\mathbf{n},1}(E, V_0) &= \begin{cases} \dfrac{12\,\tilde{k}\,k_\ell\, e^{\mathrm{i}\,\tilde{k}L}\left(q_{n_y}^2 + q_{n_z}^2\right)}{\tilde{k}^2\left(e^{2\,\mathrm{i}\,\tilde{k}L} - 1\right)\left(4\,k_\ell^2 + q_{n_y}^2 + q_{n_z}^2\right) + \left(e^{2\,\mathrm{i}\,\tilde{k}L} - 1\right)\left(q_{n_y}^2 + q_{n_z}^2\right)\left[k_\ell^2 + 4\left(q_{n_y}^2 + q_{n_z}^2\right)\right] + 6\,\tilde{k}\,k_\ell\left(e^{2\,\mathrm{i}\,\tilde{k}L} + 1\right)\left(q_{n_y}^2 + q_{n_z}^2\right)} & \text{for } E < V_0 \\ \dfrac{2\,\mathrm{i}\,\tilde{k}\,k_\ell}{\left(\tilde{k}^2 + k_\ell^2\right)\sin\left(\tilde{k}L\right) + 2\,\mathrm{i}\,\tilde{k}\,k_\ell\cos\left(\tilde{k}L\right)} & \text{for } E > V_0\,, \end{cases} \\
t_{\mathbf{n},2}(E, V_0) &= 0\,.
\end{aligned} \tag{3.12}$$

The transmission coefficient at an energy E is given by

$$T(E, V_0, \theta, \phi) = \left|t_{\mathbf{n},1}(E, V_0)\right|^2\,, \text{ where } \theta = \cos^{-1}\left(\frac{\hbar\, q_{n_z}}{\sqrt{2\,m\,E}}\right) \text{ and } \phi = \tan^{-1}\left(\frac{q_{n_y}}{k_\ell}\right) \tag{3.13}$$

define the incident angle (solid) of the incoming wave in 3d.

Preprints (www.preprints.org) | NOT PEER-REVIEWED | Posted: 5 June 2020 doi:10.20944/preprints202006.0051.v1

Peer-reviewed version available at Annals of Physics 2020, 419, 168235; doi:10.1016/j.aop.2020.168235

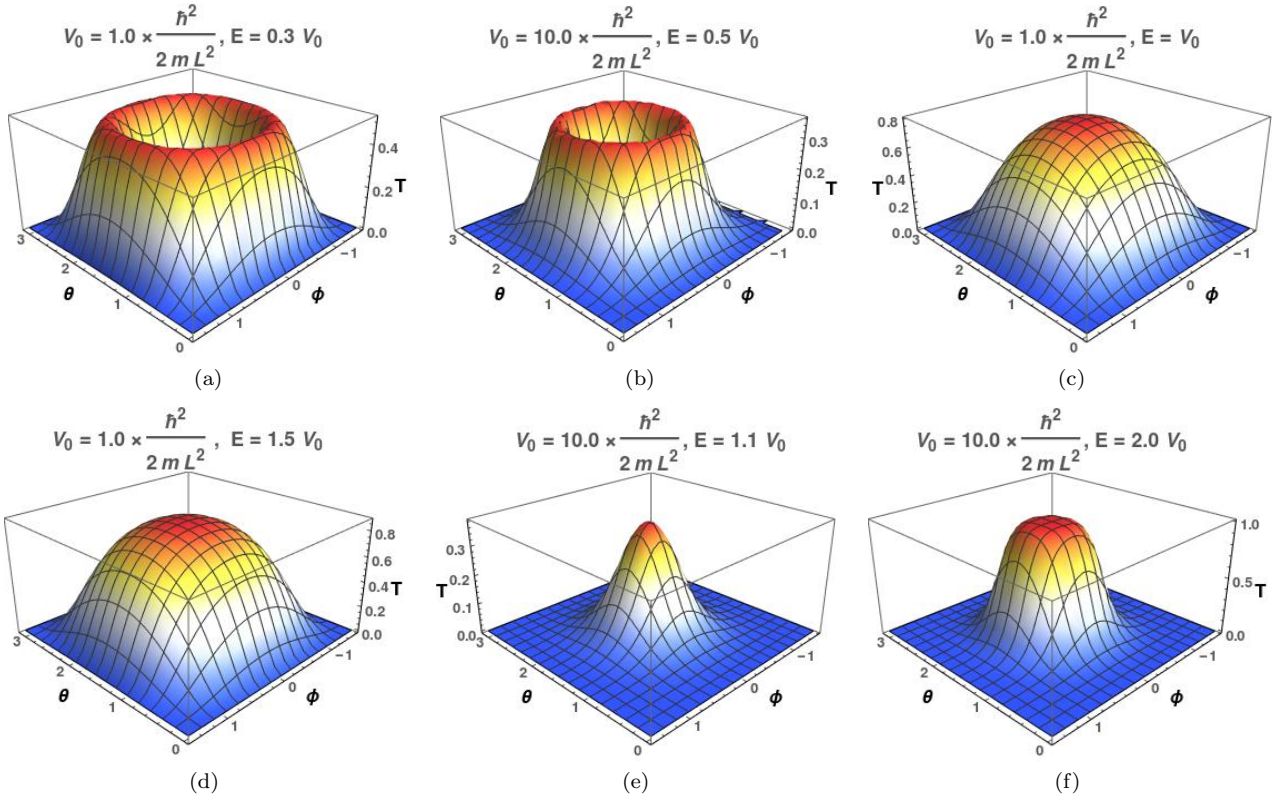

FIG. 5. Plots of the transmission coefficient (T) for $3d$ QBCP as a function of (θ, ϕ), for various values of V_0 and E.

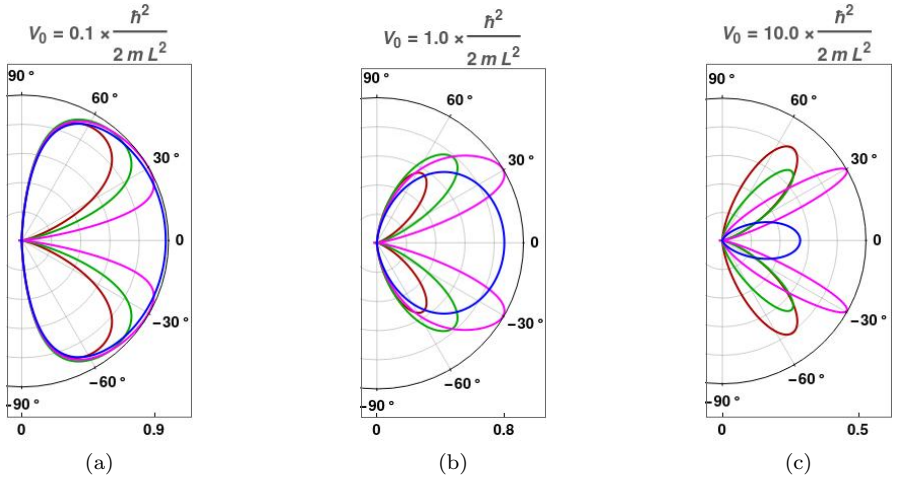

FIG. 6. 3d QBCP: The polar plots show the transmission coefficient $T(E, V_0, \theta, \frac{\pi}{2})\big|_{E \le V_0}$ as a function of the incident angle ϕ (in the $xy-$plane with no k_z-component) for the parameters $E = 0.3\,V_0$ (red), $E = 0.5\,V_0$ (green), $E = 0.8\,V_0$ (magenta) and $E = 1.0\,V_0$ (blue).

B. Transmission coefficient, conductivity and Fano factor

Again, we assume W to be very large such that $\left(q_{n_y}, q_{n_z}\right)$ can effectively be treated as continuous variables. Using $k_\ell = \sqrt{\frac{2mE}{\hbar^2}}\sin\theta\cos\phi\,, \quad n_y = \frac{W\sqrt{2mE}}{h}\sin\theta\sin\phi\,, \quad n_z = \frac{W\sqrt{2mE}}{h}\cos\theta\,, \quad dn_y\,dn_z = \frac{W^2\times 2\,m\,E}{h^2}\cos\phi\sin^2\theta\,d\phi,$ in

Preprints (www.preprints.org) | NOT PEER-REVIEWED | Posted: 5 June 2020 doi:10.20944/preprints202006.0051.v1

Peer-reviewed version available at Annals of Physics 2020, 419, 168235; doi:10.1016/j.aop.2020.168235

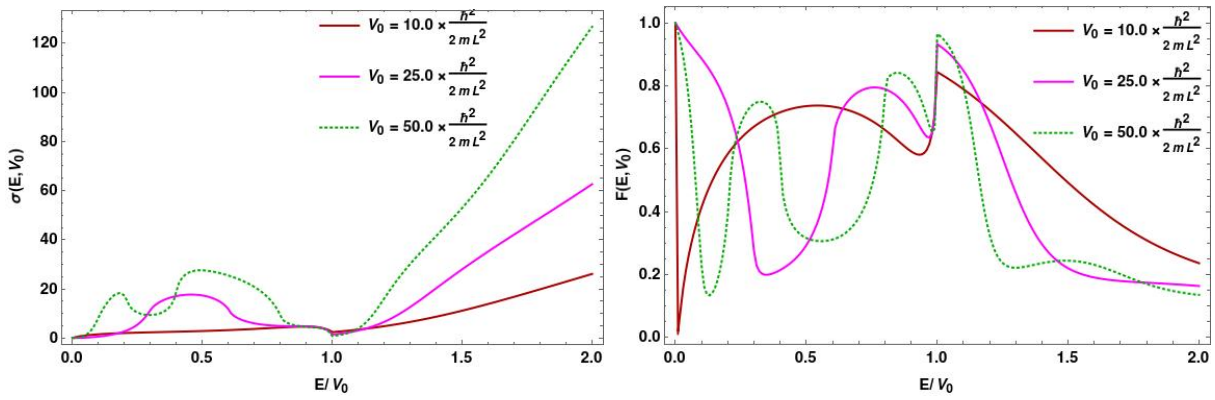

(a) (b)

FIG. 7. 3d QBCP: Plots of the (a) conductivity (σ in units of $8\pi^2$), and (b) Fano factor (F), as functions of E/V_0, for various values of V_0.

the zero-temperature limit and for a small applied voltage, the conductance is given by:[15]

$$G(E,V_0) = \frac{2\,e^2}{h}\sum_{\mathbf{n}}|t_{\mathbf{n},1}|^2 \to \frac{2\,e^2}{h}\int |t_{\mathbf{n},1}|^2\,dn_x\,dn_y = \frac{4\,\pi\,e^2\,W^2}{\hbar}\left(\frac{2\,m\,E}{\hbar^2}\right)\int_{\theta=0}^{\pi}\int_{\phi=-\frac{\pi}{2}}^{\frac{\pi}{2}} T(E,V_0,\theta,\phi)\cos\phi\sin^2\theta\,d\phi\,, \tag{3.14}$$

leading to the conductivity expression:

$$\sigma(E,V_0) = \left(\frac{L}{W}\right)^2\frac{G(E,V_0)}{e^2/h} = 8\,\pi^2\left[\frac{E}{\hbar^2/\left(2\,mL^2\right)}\right]\int_{\theta=0}^{\pi}\int_{\phi=-\frac{\pi}{2}}^{\frac{\pi}{2}} T(E,V_0,\theta,\phi)\cos\phi\sin^2\theta\,d\phi\,. \tag{3.15}$$

Note that there is a twofold degeneracy because we have two independent conduction band states, and hence an extra factor of two has been included in the expressions for G and σ. The shot noise and Fano factor can be expressed as:

$$\mathcal{S}(E,V_0) = \frac{4\,e^2\,\Phi}{h}\sum_{\mathbf{n}}|t_{\mathbf{n},1}|^2\left(1-|t_{\mathbf{n},1}|^2\right) \to \frac{8\,\pi\,e^3\,W^2\,\Phi}{\hbar}\left(\frac{2\,m\,E}{\hbar^2}\right)\int_0^{\frac{\pi}{2}} T(E,V_0,\phi)\left[1-T(E,V_0,\phi)\right]\,d\phi\,, \tag{3.16}$$

and

$$F(E,V_0) = \frac{\int_{\theta=0}^{\pi}\int_{\phi=-\frac{\pi}{2}}^{\frac{\pi}{2}} T(E,V_0,\theta,\phi)\cos\phi\sin^2\theta\,d\phi}{\int_{\theta=0}^{\pi}\int_{\phi=-\frac{\pi}{2}}^{\frac{\pi}{2}} T(E,V_0,\theta,\phi)\left[1-T(E,V_0,\theta,\phi)\right]\cos\phi\sin^2\theta\,d\phi}\,, \tag{3.17}$$

respectively. Here, Φ is the applied voltage.

As before, we express E and V_0 in units of $\frac{\hbar^2}{2\,mL^2}$, and study the behaviour of $T(E,V_0,\theta,\phi)$, $\sigma(E,V_0)$ and $F(E,V_0)$. From the expression of transmission coefficient in Eq. (3.12), it is clear that the transmission is zero at normal incidence ($\theta=\pi/2,\phi=0$), as long as $E<V_0$. This is analogous to the 2d case. In Fig. 5, we show the angular dependence of $T(E,V_0,\theta,\phi)$ in 3d plots. Fig. 6 shows the polar plots of $T(E,V_0,\pi/2,\phi)$ as a function of the incident angle ϕ for $E\le V_0$, which corresponds to $k_z=0$. Since the transmission coefficient for $E>V_0$ has the same expression both for the 2d and 3d QBCPs, the polar plots of $T(E,V_0,\pi/2,\phi)\big|_{E>V_0}$ will be identical to Fig. 3. In Fig. 7, we illustrate the conductivity $\sigma(E,V_0)$ and the Fano factor $F(E,V_0)$, as functions of E/V_0, for some values of V_0.

IV. COMPARISON WITH THE THE RESULTS FOR ELECTRONS IN NORMAL METALS

We compare the results obtained for QBCP semimetals with those in normal metals. For normal metals, we have only one electron band to consider where the Fermi energy will intersect (irrespective of the height of the barrier).

Preprints (www.preprints.org) | NOT PEER-REVIEWED | Posted: 5 June 2020 doi:10.20944/preprints202006.0051.v1

Peer-reviewed version available at Annals of Physics 2020, 419, 168235; doi:10.1016/j.aop.2020.168235

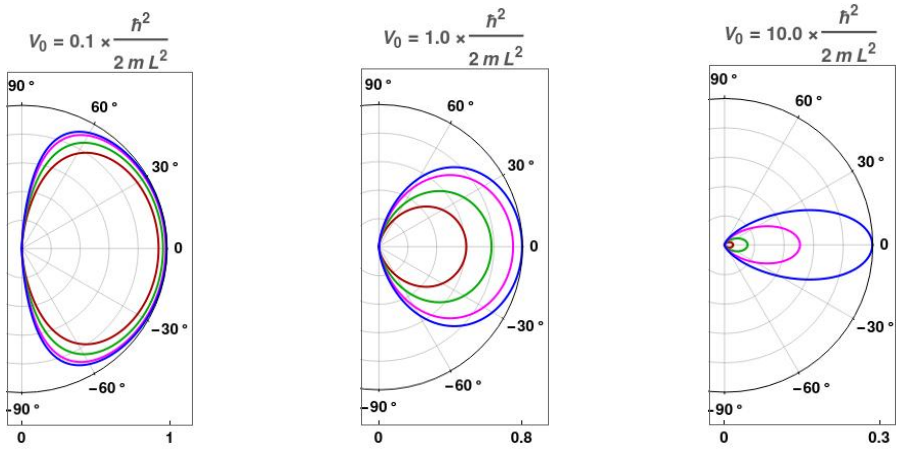

(a) (b) (c)

FIG. 8. Normal metal: The polar plots show the transmission coefficient $T(E, V_0, \phi)\big|_{E<V_0}$ as functions of the incident angle ϕ for the parameters $E = 0.3\,V_0$ (red), $E = 0.5\,V_0$ (green), $E = 0.8\,V_0$ (magenta) and $E = 1.0\,V_0$ (blue).

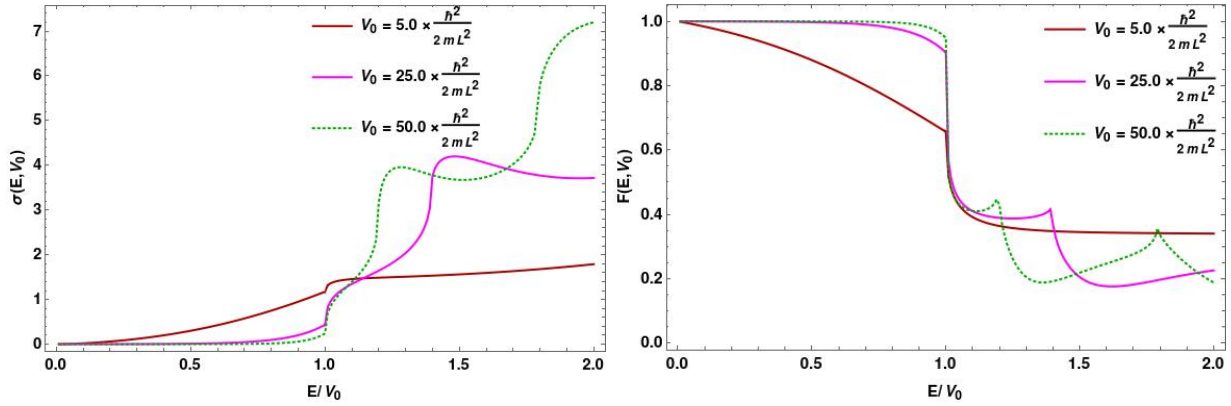

(a) (b)

FIG. 9. 2d normal metal: Plots of the (a) conductivity (σ in units of 2π), and (b) Fano factor (F), as functions of E/V_0, for various values of V_0.

Using the continuity of the wavefunctions and their x-derivatives at the two ends of the barrier, we can easily find the transmission coefficient to be always given by:

$$t(E, V_0) = \frac{2\,\mathrm{i}\,\tilde{k}\,k_\ell}{\left(\tilde{k}^2 + k_\ell^2\right)\sin\left(\tilde{k}L\right) + 2\,\mathrm{i}\,\tilde{k}\,k_\ell\cos\left(\tilde{k}L\right)}\,, \tag{4.1}$$

independent of whether $E < V_0$ or $E > V_0$. As expected, this expression varies from the QBCP case only in the $E < V_0$ regime, as whenever $E > V_0$, a quasiparticle excitation moves across the barrier in the same way as a normal metal electron does.

In Fig. 8, we show the plots of the transmission amplitude $T(E, V_0, \phi) = |t(E, V_0)|^2$ as function of the angle ϕ, for the normal metal (in the 2d case, or 3d case with $k_z = 0$). We also show the behaviour of conductivity and Fano factor for 2d and 3d normal electrons in Figs. 9 and 10 respectively. As expected, Fig. 9 differs from Fig. 4, or Fig. 10 differs from Fig. 7, only in the regions where $E < V_0$.

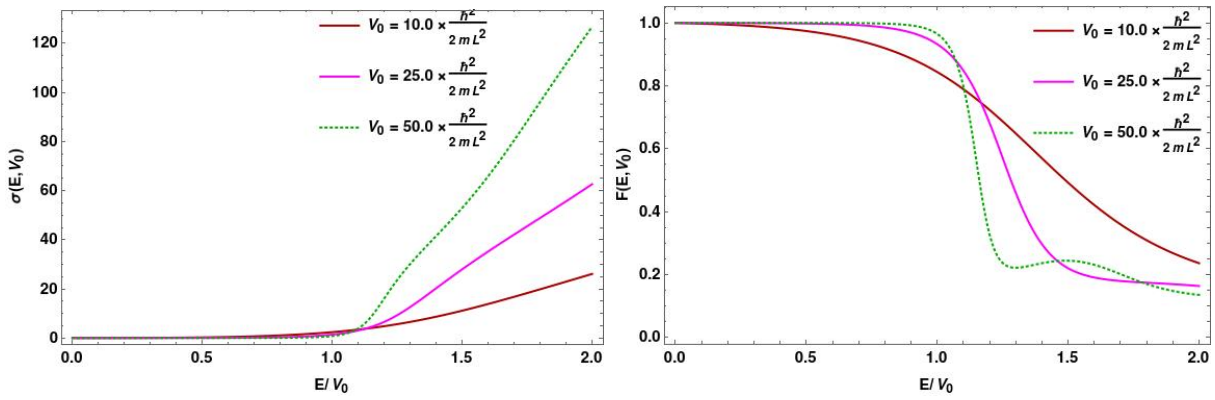

(a) (b)

FIG. 10. 3d normal metal: Plots of the (a) conductivity (σ in units of $2\pi^2$), and (b) Fano factor (F), as functions of E/V_0, for various values of V_0.

V. SUMMARY AND DISCUSSIONS

From our computations of the tunneling coefficients for the 2d and 3d QBCP semimetals, we have shown that they exhibit different characteristics than those expected for normal metals. The answers also differ from those expected for graphene[16] and three-band pseudospin-1 semimetals.[17,18] In particular, QBCPs do not exhibit either Klein or super-Klein tunneling.[18] We also note that the transport characteristics for the 2d and 3d QBCP cases show significant differences among themselves. All these observations can be used in experiments to identify the QBCP semimetals.

In future, it will be useful to look at these transport properties in the presence of disorder[21] (as has been done in the case of Weyl[22] and double-Weyl[23] nodes) and/or magnetic fields.[24] Another direction is to examine the effects of anisotropy as well as particle-hole symmetry-breaking terms. Yet another direction is to explore the time-dependent transport properties when subjected to a time-dependent potential,[25] using the Floquet scattering theory, and find out if Fano resonance can occur via quasibound states.

VI. ACKNOWLEDGMENTS

We thank Emil J. Bergholtz for useful discussions, and Atri Bhattacharya for help with the figures.

[1] K. Sun, H. Yao, E. Fradkin, and S. A. Kivelson, Phys. Rev. Lett. **103**, 046811 (2009).
[2] W.-F. Tsai, C. Fang, H. Yao, and J. Hu, New Journal of Physics **17**, 055016 (2015).
[3] I. Mandal and S. Gemsheim, Condensed Matter Physics **22**, 13701 (2019).
[4] A. A. Abrikosov, JETP **39**, 709 (1974).
[5] T. Kondo, M. Nakayama, R. Chen, J. J. Ishikawa, E. G. Moon, T. Yamamoto, Y. Ota, W. Malaeb, H. Kanai, Y. Nakashima, Y. Ishida, R. Yoshida, H. Yamamoto, M. Matsunami, S. Kimura, N. Inami, K. Ono, H. Kumigashira, S. Nakatsuji, L. Balents, and S. Shin, Nat Commun **6** (2015).
[6] E.-G. Moon, C. Xu, Y. B. Kim, and L. Balents, Phys. Rev. Lett. **111**, 206401 (2013).
[7] D. Yanagishima and Y. Maeno, Journal of the Physical Society of Japan **70**, 2880 (2001).
[8] K. Matsuhira, M. Wakeshima, R. Nakanishi, T. Yamada, A. Nakamura, W. Kawano, S. Takagi, and Y. Hinatsu, Journal of the Physical Society of Japan **76**, 043706 (2007).
[9] A. A. Abrikosov and S. D. Beneslavskiĭ, Soviet Journal of Experimental and Theoretical Physics **32**, 699 (1971).
[10] I. Boettcher and I. F. Herbut, Phys. Rev. B **93**, 205138 (2016).
[11] J. M. Luttinger, Phys. Rev. **102**, 1030 (1956).
[12] S. Murakami, N. Nagosa, and S.-C. Zhang, Phys. Rev. B **69**, 235206 (2004).
[13] M. Salehi and S. Jafari, Annals of Physics **359**, 64 (2015).
[14] J. Tworzydło, B. Trauzettel, M. Titov, A. Rycerz, and C. W. J. Beenakker, Phys. Rev. Lett. **96**, 246802 (2006).

[15] Y. Blanter and M. Büttiker, Physics Reports **336**, 1 (2000).
[16] M. I. Katsnelson, K. S. Novoselov, and A. K. Geim, Nature Physics **2**, 620 (2006).
[17] A. Fang, Z. Q. Zhang, S. G. Louie, and C. T. Chan, Phys. Rev. B **93**, 035422 (2016).
[18] R. Zhu and P. M. Hui, Physics Letters A **381**, 1971 (2017).
[19] L. Janssen and I. F. Herbut, Phys. Rev. B **92**, 045117 (2015).
[20] I. F. Herbut, Phys. Rev. B **85**, 085304 (2012).
[21] R. M. Nandkishore and S. A. Parameswaran, Phys. Rev. B **95**, 205106 (2017); I. Mandal and R. M. Nandkishore, *ibid.* **97**, 125121 (2018); I. Mandal, Annals of Physics **392**, 179 (2018).
[22] B. Sbierski, G. Pohl, E. J. Bergholtz, and P. W. Brouwer, Phys. Rev. Lett. **113**, 026602 (2014).
[23] B. Sbierski, M. Trescher, E. J. Bergholtz, and P. W. Brouwer, Phys. Rev. B **95**, 115104 (2017).
[24] C. Yesilyurt, S. G. Tan, G. Liang, and M. B. A. Jalil, Scientific Reports **6**, 38862 (2016).
[25] R. Zhu and C. Cai, Journal of Applied Physics **122**, 124302 (2017).